International Journal of Science and Research (IJSR)
ISSN: 2319-7064
SJIF (2022): 7.942

Performance Analysis of 50MW Parabolic Trough Solar Thermal Power Plant under Makkah City Climatological Conditions

Talal M. AlSufyani[1], Abdulmajeed S. Al-Ghamdi[2]

[1]Department of Mechanical Engineering, College of Engineering and Islamic Architecture, Umm Al-Qura University, Al Abdeyah, 715, Makkah, 21955, Saudi Arabia
Corresponding author Email: *talal.so77[at]gmail.com*

[2]Department of Mechanical Engineering, College of Engineering and Islamic Architecture, Umm Al-Qura University, Al Abdeyah, 715, Makkah, 21955, Saudi Arabia
asaalghamdi[at]uqu.edu.sa

Abstract: ***This study examines the energetic and exergetic performance of a concentrated solar power (CSP) plant that uses parabolic trough collectors (PTC) based on Makkah Climatological Conditions. by utilizing steam power block with six heaters and turbine extraction lines, three heaters also are running at high pressure., letting the remaining three be operated at low pressure along with a deaerator, The (CSP)plant produces 50 MW of electricity. Additionally, a calculation model was created to predict the plant's energy generation utilizing the proposed CSP plant concept design and solar irradiation data of Makkah city. Investigations are made into the study of the first as well as second laws of the cycle thermal in addition to exergy efficiency. The results show that with LS-3 collector type a 246, 885$m^2$of aperture area and a full plant area of 976, 416 $m^2$is enough to cover annual electricity of 117.2 GWh. The solar field outlet temperature is 392^{0}C with a corresponding daily energy efficiency of 65.6%.The daily average power cycle energy and exergy efficiencies are found to be 39.4%, and 33.5%, respectively.***

Keywords: Solar energy, Energy, Exergy, Parabolic trough collector, efficiency

1. Introduction

The Kingdom of Saudi Arabia is one of the large countries in the middle east, and with a total area of around 2, 000, 000 square kilometers, makes up about four fifths of the Arab Peninsula. The total Electricity consumption from all sectors by Saudi Arabia in 2020is recorded to be 289.32 TWh [1]. It's domestic recoverable energy resources are growing to cope with the increasing demands of electricity by the population. certainly, by this work time it doesn't satisfy the full demands, but it going to cover a high portion of it according to 2030 vision strategic plan, with a target of having 58.7 GW of renewable energy by 2030, of which 40GW PV, 16GW Wind and 2.7GW Concentrated solar thermal power (CSP)[2], which is the main scope of this study.

The use of concentrated solar thermal power for utility scale energy production is increasing. Parabolic troughs, solar towers, and dish Sterling technology are the three primary divisions within concentrating solar thermal power.

Parabolic trough power plants are regarded as the most popular viable option. From 1984 through 1990, Luz International Limited laid the groundwork for commercial parabolic trough power plants. In California, nine solar facilities with capacities varying between 30 and 80 megawatts (MWe) were built and are still operational today. Figure 1 shows parabolic troughs collectors of the SEGS plant, SEGS VI, which has been the subject of published studies on parabolic trough power plants. The information provided for the 35 MWe SEGS VI plant was used to create the proposed study design and modified for Makkah city climatological conditions in Saudi Arabia.

Figure 1: Parabolic troughs collectors of the SEGS plant [3]

From 1984 to the time of this work the research and development of concentrated solar power (CSP) plants have evolved and grown rapidly. As a result of this growth, the CSP technology became mature enough to be considered a highly reliable renewable energy power generation system, thus becoming more cost-effective from a business point of view.

Many studies have been conducted by researchers to study the possibility of converting solar energy into electrical energy due to the abundance of solar radiation in various places. PV cells were studied economically by Woditsch [4]. The study is based on the assumption that market volumes will double every four years, with cost reductions of 20% for

each doubling. This study predicts a 50 percent cost decrease over the next 10, assuming the same pace of growth. However, in hot places such as the Middle East, summer temperatures are quite high, and this high temperature has a negative impact on the PV system's energy generation. Because of their dark tint, the cell temperature of PVs is much higher than the ambient temperature[5]. On the contrary, Enermodal [6], is from the other hand, conducted a cost-benefit analysis for a parabolic trough collector, comparable to Woditsch [4]. When the market volume is doubled, the outcome reveals a cost decrease of 12%. In the following decade, this will result in a 40% cost decrease.

Lippke (1995) used EASY simulation software to create an extensive thermodynamic analysis model of the SEGS VI solar field in addition to the power block[3]. The goal of his work was to simulate the behaviour of the system under partial load conditions (like winter season and cloudy days). Back-calculating turbine stages efficiencies and the overall conductance (UA) values for all of the installed heat exchangers in the power and solar block is done in his model using chosen state points from the plant description. Hourly CSP plant data for both a summer day and a winter day were used for model validation.

Many private parabolic trough power plant models exist, like as Solar Millennium's PC Trough, however they are not publicly available. Patnode [7] used Engineering Equation Solver, EES, and TRNSYS to run a comprehensive simulation of SEGS VI.

Joseph E. Kopp study[8] investigated the indirect thermal storage designs for solar parabolic trough power plants, and the effect of several designs starting with a CSP plant working in transient without thermal storage, then the conventual thermal storage two tanks with molten salt cycle suppling the HTF with the required energy for the steam train, the focus of Joseph E. work was in utilizing the thermal storage fluid (Molten salt) to supply power cycle steam train with the required energy instead of the usual HTF. In this work, the equations and design values supplied by Patnode and Joseph were utilised, therefore, the presented design will evaluate the Solar field and the power cycle performance for thermal storage future studies.

2. An overview of the Middle East CSPP developments

The Middle East area considered a high potential for concentrating solar power, where in UAE at the city of Madinat Zayed, which is 120 kilometers south-west of Abu Dhabi, the Shams solar power station is being constructed. The Shams 1 solar project's first phase of construction got under way in July 2010, and it started operating in March 2013.It has a 100-megawatt electricity production and a footprint of 2.5 square kilometers. 768 parabolic trough collectors in the solar field produce clean, renewable electricity, enough electricity to power 62, 000 houses[9].

Lately in 2018, Shagaya Renewable Energy Park, a 50 Mwe CSP parabolic trough solar power Plant, finished the construction stage and began operation in shagaya, Kuwait. TSK constructed and operates the plant. Shagaya CSP Plant will be producing 180GWh/year with a total area of 250 hectares and avoiding the emission of more than 81000 tons of CO2/year[10].

The largest single-site concentrated solar power plant in the world, the 950 MW hybrid project (700 MW CSP & 250 MW PV) of the Mohammed Bin Rashid Al Maktoum Solar Park harvests solar energy using a state-of-the-art combination of a central tower and a parabolic trough concentrated solar power (CSP) technologies. A levelized tariff of US $7.30 cents per kilowatt-hour will be used for the project's power delivery. The facility will help Dubai Clean Energy Strategy 2050 achieve its goal of using 25 percent clean energy by 2030 and will enable a CO2 reduction of 1.6 million tons [11].

3. Electricity consumption of Makkah City and Umm Al-Qura University

The amount of electricity consumed in Saudi Arabia in 2018 was around 289.8 terawatt hours TWh, a minor increase of 0.42 percent above the 288.6 TWh consumed in 2017. Peak electricity demand was 61.7 gigawatts (GW) in 2018, down 1.5 percent from 62.1 GW in 2017, while power generation capacity fell to 68.8 GW in 2018 from roughly 70 GW in 2017.[1]

Umm Al-Qura University on the other hand has recorded in 2020 a total electricity consumption of 200 GWh, and that include all the university campuses. The main campuses specifically recorded a 100MW of electricity consumption.

4. Solar irradiation on Saudi Arabia and the proposed CSP Plant site selection

Direct and diffuse components exist in sun irradiation, which is the energy source for solar power plants. Only direct solar irradiation has the ability to be concentrated and thus using that for electricity generation by the CSP plant. Solar radiation measurement has the ability to be done in a variety of ways, with ground-based and satellite-based information being the most common. Solar irradiation potential over large areas, such as specific counties or states, is determined using satellite information. The constant of the extraterrestrial is decreased by clouds, and dust, fog, and more atmospheric factors monitored using meteorological satellites to get the figures for solar irradiation. For further in-depth site analyses, ground-based data is used. Only on the basis of this data an intensive planning in addition to thorough project development, including energy gross forecasting, can be done.

Umm Al-Qura university has cooperated with K-A-Care in 2010to install Tier-1 research ground-based solar station in Makkah city as part of Saudi Arabia initiative to fund a lot of solar projects and approximately 53 stations installations across the country as shown in

Figure 2

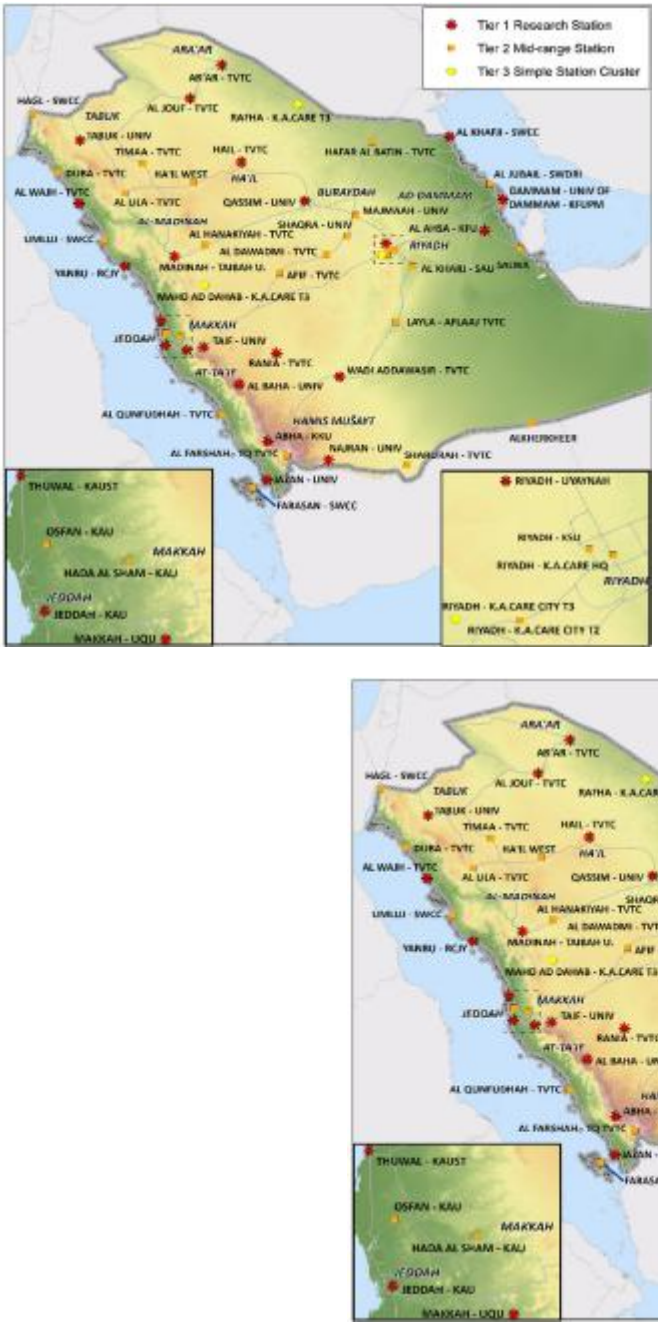

Figure 2: Solar monitoring network design.[12]

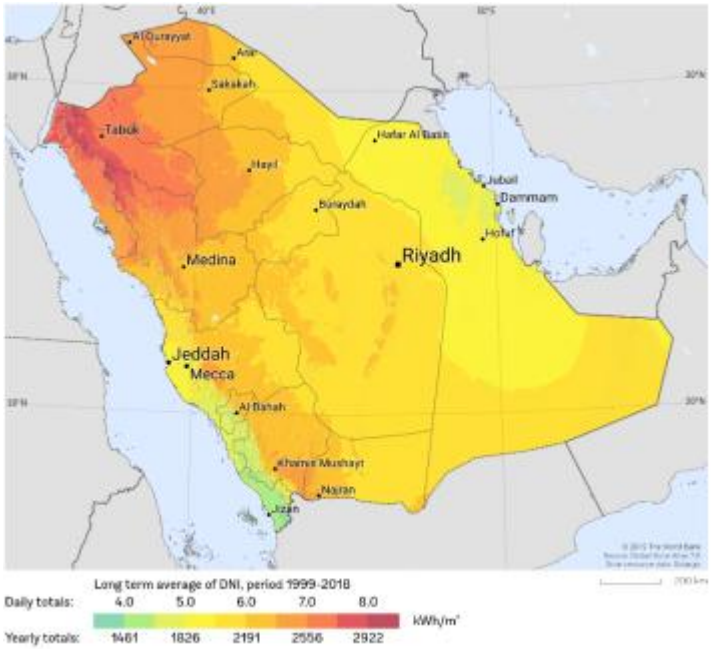

Figure 3: Saudi Arabia's average daily total of direct normal irradiation in square meters is shown on the solar map

A detailed analysis of the direct solar irradiation over Makkah city which have the configuration listed in Figure **4:** Direct normal irradiance DNI over Makkah city

Table 1 is a significant step to evaluate the feasibility of the proposed plant design electricity generation efficiency. The operation and installation of CSP plant is economically viable when its higher than the average yearly direct normal irradiation of 2000 kWh/m^2annually [13]. Figure 4 has been generated from the year 2020 solar irradiation data of Makkah city by employing Umm Al-Qura University Tier-1 research ground-based solar station. It is clear that Makkah city has received a daily irradiance around 1000-1100 W/m^2 on summer season, while this amount will naturally decrease to around 750 –900W/m^2 on other seasons. The analysis of collected weather data for the study selected site shows that Makkah city receive an average annual direct normal irradiation (DNI) 2390.22 kWh/ m^2 Which make concentrated solar power plants in Makkah city is economically viable option for power generation.

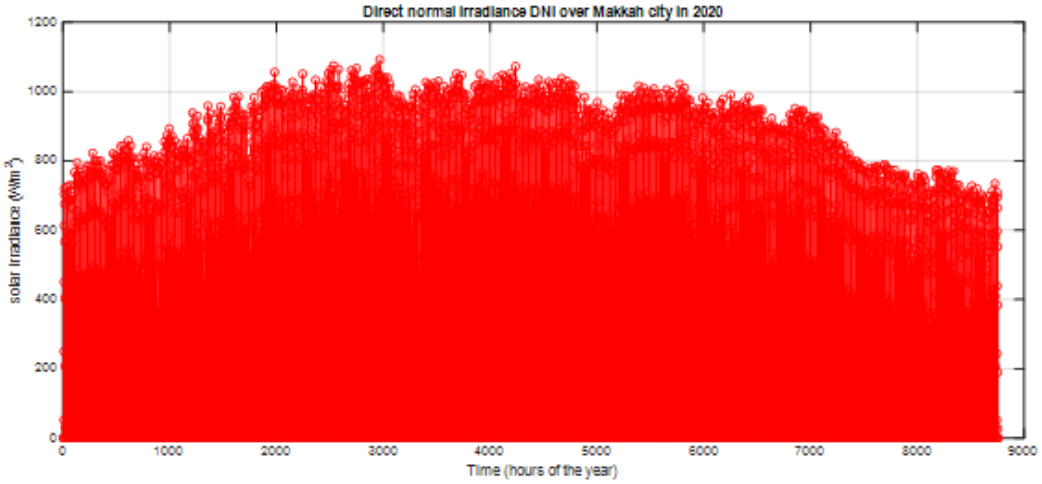

Figure 4: Direct normal irradiance DNI over Makkah city

Table 1: Makkah city Site configuration for the proposed CSP plant

Parameter	Value
Average annual direct normal irradiation (DNI)	2390.22 kWh/m^2
Longitude	21.3891° N
Latitude	39.8579° E
Altitude	277 m

5. The Proposed Parabolic trough Solar Power Plant

The proposed parabolic trough solar power plant is consisting of three subsystems, which are integrated with one another: the collector solar field, and the heat transfer fluid (HTF), in addition to the power block. Collector loops are organized in parallel as demonstrated in Figure 6 in the collector field. Each loop is made up of collectors that are connected in a loop. The solar irradiation is concentrated

into a focal line by collectors, which heats up the heat transfer fluid. The collectors then must be rotated by a solar tracking system in order to concentrate the sunlight from sunrise through sunset

The HTF system with Therminol VP-1 as main fluid is utilized to transfer the heat. Heated HTF with a temperature of roughly 395°C is transmitted from the collectors into the power block. After distributing the heat to generate steam, the heat thermal fluid is returned directly to the collectors at roughly 293°C. Pumps, pipelines, valves, and vessels are all necessary components for HTF circulation. The melting temperature of heat thermal fluid is 12 degrees[14].

The power block as designed in Figure 8 change the heat from the heat thermal fluid to superheated steam, the turbine-generators produces electrical power using the supplied superheated steam, whereas in a direct steam generating (DSG) power plant, the turbine-generator is driven by superheated steam. An advanced steam cycle with two reheat in addition to also two turbine extraction, three high-pressure heaters and three low-pressure heaters with a deaerator is used to increase power cycle efficiency.

The following presumptions serve as the foundation for the conceptual design for the proposed CSPP:

- The year 2020solar irradiation information and data for over Makkah city byTier-1 research ground station is used.
- No use of fossil-fueled steam boiler
- No use of thermal storage.

A auxiliary fossil-fossil-fueled boiler is not included in this original concept. A backup system should be included in the full project preparation to extend the time of plant operation availability. It could be a thermal storage system or a fossil-fueled boiler. The collector field design is heavily influenced by the collector type chosen.

Luz developed the Luz System Three (LS-3) SCA Shown in Figure 5, which was used mostly at larger facilities to increase performance based on lessons learned from solar electric generating system power plants. The LS-3 Type collector is the collector type used for this study. Because it is the most popular and well-known collector design in solar power generating facilities, it is larger than the LS-1 and LS2 collectors. It follows the sun from east to west and operates on a horizontal north-south axis. The stainless-steel receiver tube has a selective coating applied to it to improve its ability to absorb incoming radiation. In order to minimize convective heat losses, the receiver is additionally encased with a glass evacuated tube with a 66 mm inner diameter. Table 2 contains specifics on the LS-3 Solar collector.

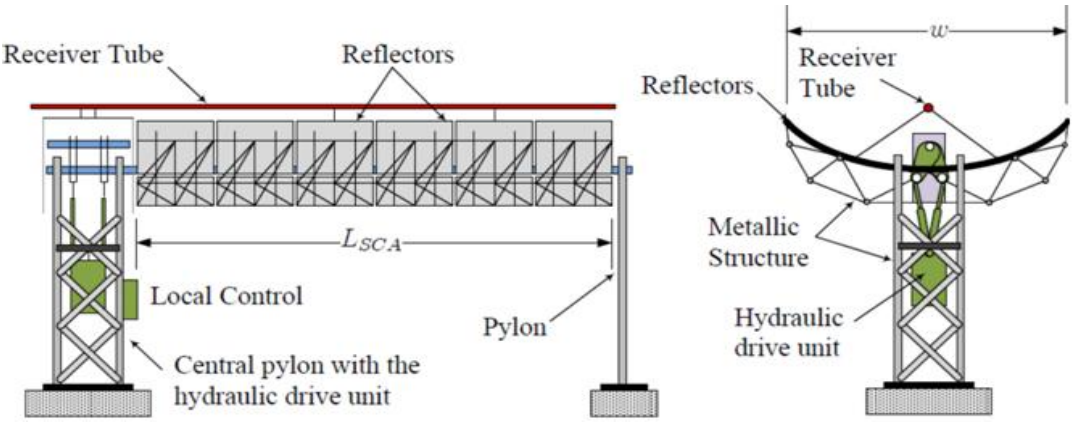

Figure 5: Layout of LS-3 solar collector assembly ("SCA") [15]

In order to prevent the decomposition of the synthetic oil (Therminol VP-1) used in the collector loops and to maintain the outlet heat transfer fluid below 393°C, the parabolic collector technology is categorized as a medium temperature system.

Table 2: Luz System Three (LS-3) Solar collector characteristics. [16, 17].

Parameter	Value
Year	1989
Area	545 m^2
Aperture width	5.76 m
Altitude	277 m
The Diameter of the Receiver	0.07m
The Ratio of Concentration	82:1
The Optical Efficiency	0.8
The Absorptivity of Receiver	0.96
The Reflectivity of the Mirror	0.94
Receiver Emittance	0.19

6. Design and modeling of solar parabolic trough collector field

Based on the above-mentioned presumptions, CSPP was designed with the layout shown in

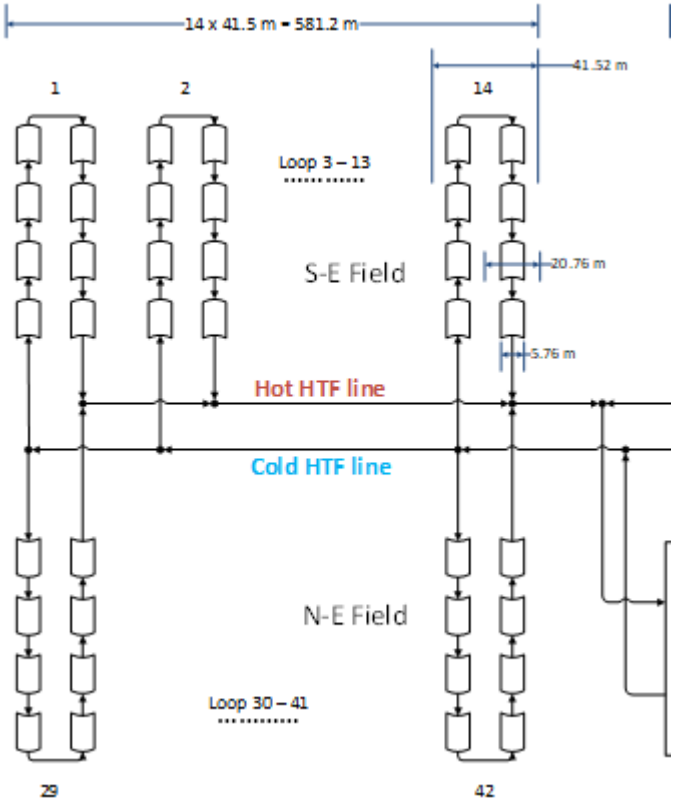

Figure the Design point Parameters listed in Table 3. With a land total area of 976, 416 m^2 and an aperture of 246, 885 m^2, the proposed plant would have a fully base load power capacity of 50 MWea56 looped LS-3 collectors and a total 453 in number. The total-load hrs are anticipated to be 2345 hour, and the solar plant is anticipated to produce around 117 GWh annually evaluated on the total solar intensities DNI at the project's location in Makkah city, Saudi Arabia.

Table 3: Design point Parameters for the proposed CSPP

Plant capacity	50 MW
Collectors' number	453
Type of the collector	LS-3
Loops number	56
Aperture area	246, 885 m^2
Total land area use	976, 416 m^2
Total-load hours	2345
yearly electricity	117.2 GW h

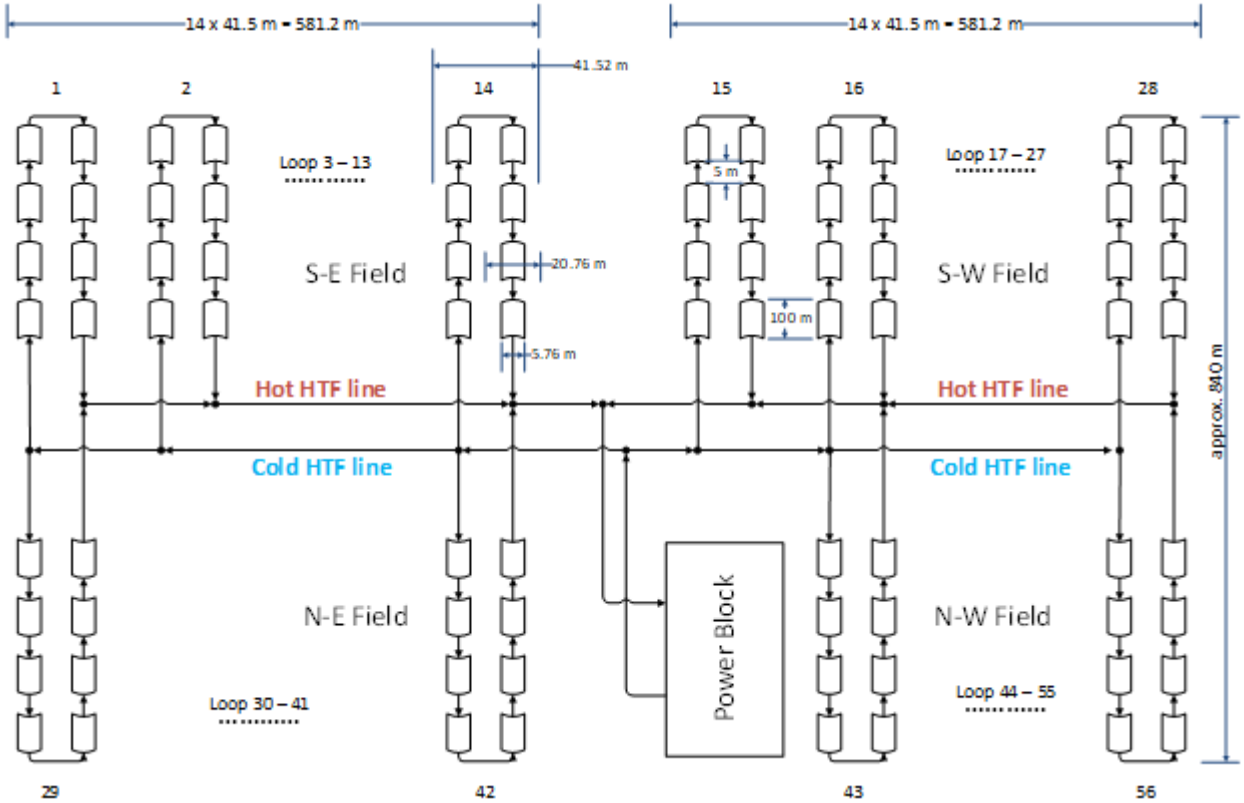

Figure 6: Schematic of the proposed concentrated solar power plant

With a low inlet temperature of 293 °C and a high output temperature of about 390 °C, the temperature gross of heat thermal fluid rise through the solar field during peak summer times is on the value of 100 °C. In order to calculate the HTF temperature leaving the solar field, the solar collector field is modeled as a component within MATLAB

Simulation. Figure 7 displays the designed solar field model simulation flow diagram.

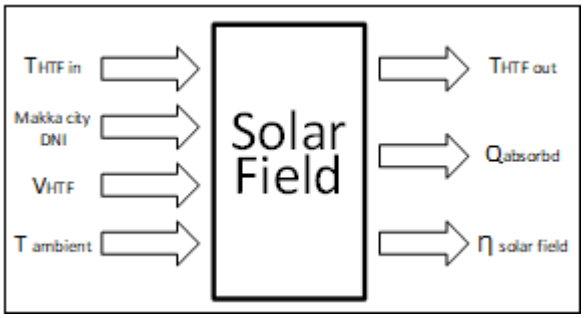

Figure 4: Solar field component information flow diagram.

Equations 1-3 define the thermal parameters of the used HTF (Therminol VP-1) as functions of temperature. These properties were chosen from the SAM [18] source code. The relationship between temperature and enthalpy is also included in equation 4.

$$cp(T) = 1000(1.509 + 0.002496T + 0.0000007888T^2)[\text{J/kg/K}] \quad (1)$$

$$k(T) = 0.1381 - 0.00008708\,T - 0.0000001729\,T^2[\text{W/m/K}] \quad (2)$$

$$h(T) = 1000(-18.34 + 1.498T + 0.001377T^2)[\text{J/kg}] \quad (3)$$

$$T(h) = -0.0000000000158\,h^2 + 0.0006072\,h + 13.37[^{\circ}\text{C}] \quad (4)$$

The output of the solar field will include the HTF's outlet temperature, energy absorption rate, and instantaneous collector field efficiency. There are three steps in the process of estimating the solar field outlet temperature. The solar energy that is absorbed by the HTF across the absorber pipe is described as the absorbed radiation, or $\dot{Q}_{absorbed}$. After being corrected for incidence angle, in addition to row shading, availability of solar fields, the cleanliness of the collector, and other factors, the absorbed irradiance will represent a percentage of the direct normal irradiance.

The effective energy gain of the HTF, collected Q, is demonstrated by a straightforward energy balance to equal the difference between the absorbed sun radiation and the heat loss percentage of the receiver. Calculating the HTF exit enthalpy requires knowledge of the HTF's useful energy gain and the fluid's entering enthalpy. The HTF's outlet temperature will then be calculated using the field's exit enthalpy.

The calculations of absorbed radiation, the heat loss of the receiver, and solar field exit temperature is demonstrated below in equation 5–9[7].

$$\dot{Q}_{absorbed} = DNI \cdot \cos(\theta) \cdot IAM \cdot RowShadow \cdot \eta_{opt} \quad (5)$$

Where:

DNI-= DNI [Watt/m^2]

θ-= Incidence Angle [degree]

IAM-= Incidence angle modifier

$RowShadow$ -= Performance parameter that takes into account the mutual shadowing of parallel collector rows in the morning and the evening

η_{opt} -=Optical efficiency that represent losses due to mirror accuracy

The only insolation that can be focused and used to warm the absorber tubes is that which is directly normal to the collection surface. The angle between a beam's emission on a surface and the plane perpendicular to that surface is represented by the angle of incidence θ.

According to Duffie and Beckman (1991)[19], the angle of incidence for a rotating plane on a horizontal north-south axis while continuously tracking to the west is as follows:

$$\cos\theta = \sqrt{cos^2\theta_z + \cos^2\delta \sin^2\omega} \quad (6)$$

The performance of the collectors will be significantly impacted by the angle of incidence, which will change during the day (and the year).Figure illustrates a day the angle of incidence and the azimuth angles over Makkah city.

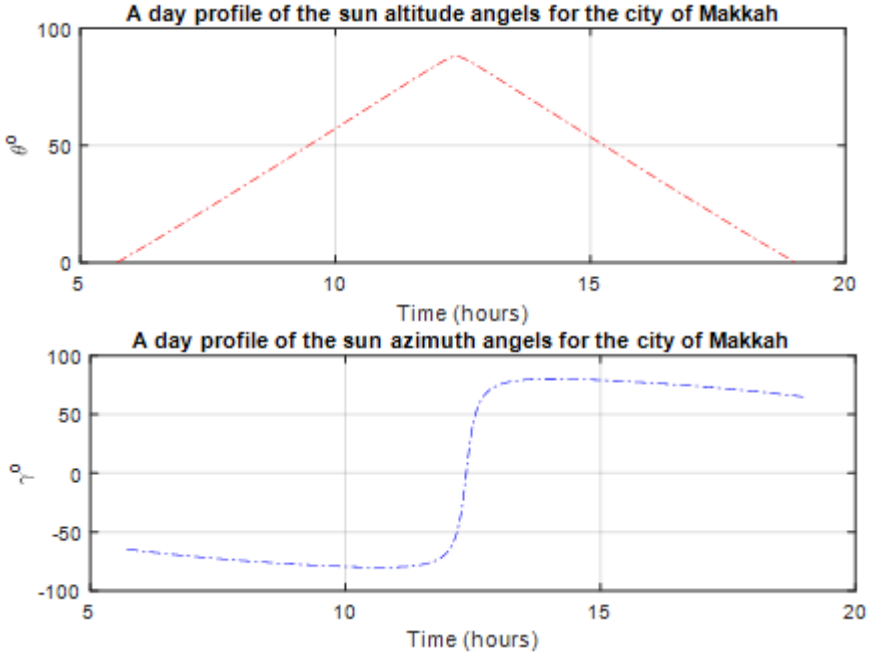

Figure 8: The altitude angels and the azimuth angels over Makkah city during the day.

These additional losses due to absorption and reflection are adjusted by the incidence angle modifier (IAM). A specific collector type's experimental data is empirically fitted with the incidence angle modifier.

Separating the losses within the available radiation caused by the incidence angle itself from reflection or absorption adjustments that tied to the angle of incidence is desirable. The incidence angle modifier experimental data (K)for the LS-3 collector type is based on Mokheimer LS-3 study in 2014[20].

According to Dudley et al[21]., the incidence angle modifier is used for this study as the incidence angle modifier divided by the cosine of the incidence angle:

$$IAM=\frac{K}{\cos(\theta)}=1+0.000884\cdot\frac{\theta}{\cos(\theta)}-0.00005369\cdot\frac{\theta^2}{\cos(\theta)} \quad (7)$$

Due to morning and evening shading of parallel rows as well as end losses from the heat collector element, the positioning and design of the collector troughs and HCEs may result in additional losses, and lowering their collector performance.

This loss is named "Row Shadow ratio" and can be calculated using the field's arrangement of collectors, the incidence angle, and the geometry of the solar zenith angle as shown in equation 8.

$$RowShadow=\frac{W_{eff}}{W}=\frac{L_{spacing}}{W}\cdot\frac{\cos(\theta_z)}{\cos(\theta)} \quad (8)$$

Using energy equations, a thermodynamic analysis of each component in the proposed system is presented. The analyses are detailed below. The heat transfer analysis approach presented by Beckman, 1980[19], The useful energy rate from the collector is defined as:

$$\dot{Q}_u=A_{ap}F_R\left(S-\frac{A_r}{A_{ap}}U_L(T_{ri}-T_o)\right) \quad (9)$$

where A_{ap} is the aperture area, A_r is the receiver area, F_R is the heat removal factor, S is the heat absorbed by the receiver, and U_L is the solar collector overall heat loss coefficient, and T is the temperature. The subscripts o and ri refer to the ambient and receiver inlet, respectively. The heat absorbed by the receiver is defined as:

$$S=G_b\eta_r \quad (10)$$

Where G_b is the direct radiation heat and η_r is the receiver efficiency which is defined as:

$$\eta_{opt}=\rho\tau\alpha\gamma K\gamma \quad (11)$$

Where (ρ) reflectivity of mirror, (τ) transmittance of glass cover, (α) absorbing factor, (γ) intercept factor, $(K\gamma)$ incidence angle modifier with Rb = $\cos\theta/\cos\theta_z$. The heat removal factor is defined as:

$$F_R=\frac{\dot{m}_rCp_r}{A_rU_L}\left[1-\exp\left(\frac{-A_rU_LF_1}{\dot{m}Cp_r}\right)\right] \quad (12)$$

Where m_r is the mass flow rate through the receiver and $F_1=F'$ is the collector efficiency factor and defined as:

$$F_R=\frac{U_o}{U_L}=F'=\frac{1/U_L}{\frac{1}{U_L}+\frac{D_o}{h_{htf}D_i}+\left(\frac{D_O}{2k}\ln\frac{D_o}{D_i}\right)} \quad (13)$$

where, h_{htf} is Fluid Heat transfer convection coefficient. To avoid the critical value of heat loss, the solar collector overall heat loss coefficient between the ambient and the receiver is defined as:

$$U_L=\left[\frac{A_r}{(h_{c,ca}+h_{r,ca})A_c}+\frac{1}{h_{r,cr}}\right]^{-1} \quad (14)$$

The radiation heat coefficient between the ambient and the cover is defined as:

$$h_{r,ca}=\varepsilon_{cv}\sigma(T_c+T_a)(T_c^2+T_a^2) \quad (15)$$

where ε_{cv} is the emittance of the cover, and σ is Stefan-Boltzmann constant. The radiation heat coefficient between the receiver and the cover is defined as:

$$h_{r,cr}=\sigma\frac{(T_c+T_{a,av})(T_c^2+T_{r,av}^2)}{\frac{1}{\varepsilon_r}+\frac{A_r}{A_c}\left(\frac{1}{\varepsilon_{cv}}-1\right)} \quad (16)$$

where the subscript av stands for the average value and ε_r represents the receiver's emittance. The following formula represents the convective heat loss coefficient between the cover and ambient:

$$h_{r,ca}=\sigma\left(\frac{Nus\,k_{air}}{D_{c,o}}\right) \quad (17)$$

Using iteration, the temperature of the cover can be calculated using this equation:

$$T_c=\left(h_{r,cr}T_{r,a}+\frac{A_c}{A_r}(h_{c,ca}+h_{r,ca})T_o\right)/\left(h_{r,cr}+\frac{A_c}{A_r}(h_{c,ca}+h_{r,ca})\right) \quad (18)$$

where Nus is the Nusselt number and k_{air} is the thermal conductivity of the air. The thermal efficiency of the solar collector is therefore written as:

$$\eta_{field}=\frac{Q_{absorbed}}{DNI} \quad (19)$$

By using equation 5 to determine the $\dot{Q}_{absorbed}$ which is the amount of heat will be supplied to the power cycle Figure 9 shows the measured direct normal Irradiation above Makkah city against the simulated absorbed solar energy through the HTF from the 1st day of August to the 7th.

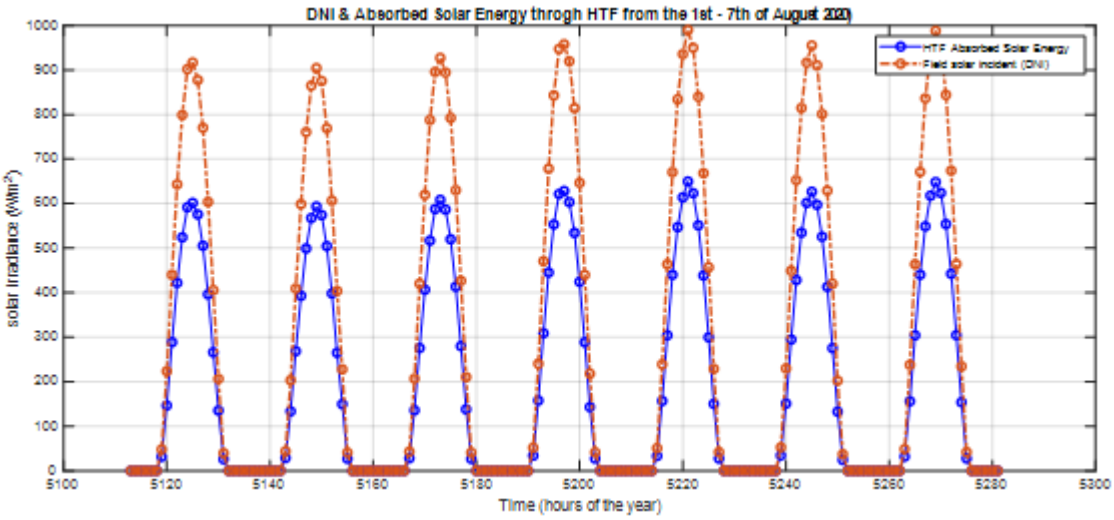

Figure 9: DNI & Absorbed Solar Energy through HTF from 1 Aug 2020 to 7 Aug 2020

On the other hand,

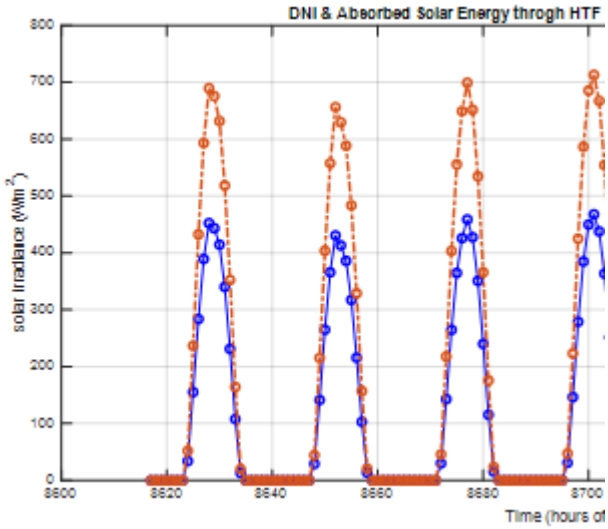

Figure shows the measured direct normal Irradiation above Makkah city against the simulated absorbed solar energy through the HTF from the 25th day of December to the 31th.

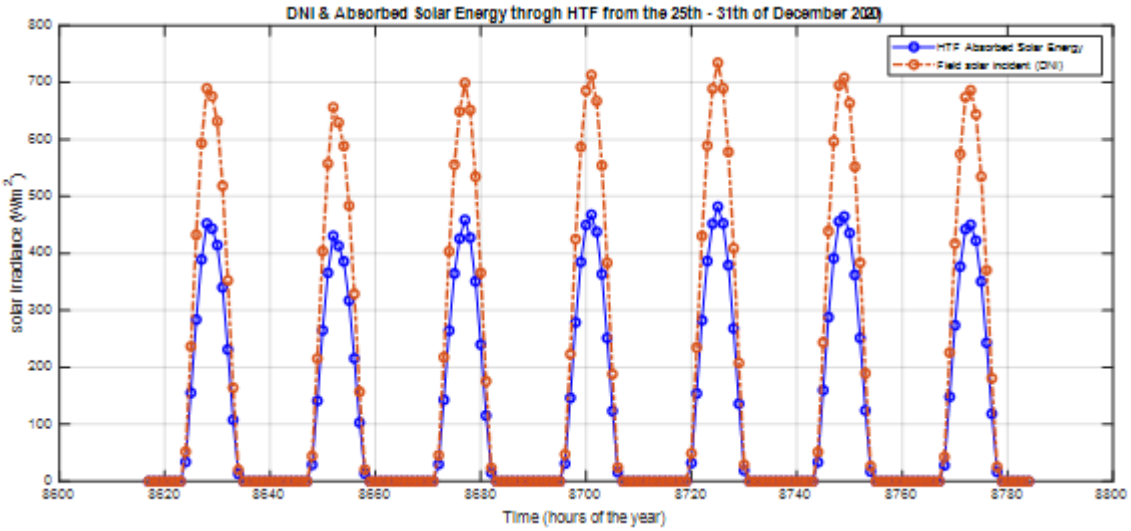

Figure 10: DNI & Absorbed Solar Energy through HTF from the 25th-31th of December 2020).

With little variations in the fluid's potential and kinetic energy across the field, it is presumed that the field is

operating at steady state. To calculate the change in fluid enthalpy from the solar field's intake to its exit, multiply the heat transfer fluid energy gained from the field by the total aperture area and divides the result by the mass flow rate of the HTF across the field as shown in Equation 20:

$$\Delta h_{field} = \frac{\dot{Q}_{absorbed} \cdot Width \cdot L_{SCA} \cdot N_{SCA}}{\dot{V}_{HTV} \cdot \rho(T_1)} \qquad (20)$$

Where:

Δh_{field} = enthalpy change of the HTF from solar field inlet to its outlet [Joule/kg]

N_{SCA} = number of SCA in the solar field

$\dot{V}_{HTV}$ = volumetric flow rate of the solar field inlet heat thermal fluid [m^3/s]

$\rho(T_1)$= HTF density at the inlet of the solar field, measured at the inlet temperature [kg/m^3]

The HTF fluid's enthalpy at the solar field output is the same as its enthalpy at the field's input as shown in equation 3 plus any change between those two points Therefore equation 9 below will result with the output enthalpy:

$$h_{out} = h_{in}(T_1) + \Delta h_{field} \qquad (21)$$

Where the enthalpy is returned in [J/kg] and the temperature must be evaluated in degree. The enthalpy of the heat transfer fluid is assumed to change with pressure only slightly. Figure 11demonstrates the enthalpy change through the solar field starting from sunrise time until the field designed peak temperature.

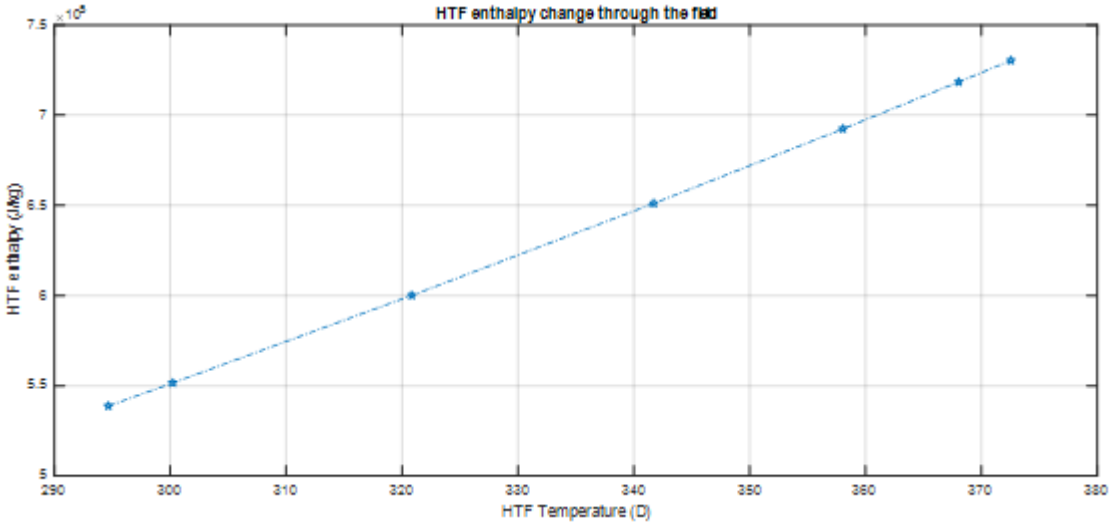

Figure 5: HTF Enthalpy Change through the solar field.

Finally, a temperature-enthalpy correlation for the HTF can be used to determine the fluid's temperature. Regarding Therminol VP-1 as shown in equation 4.

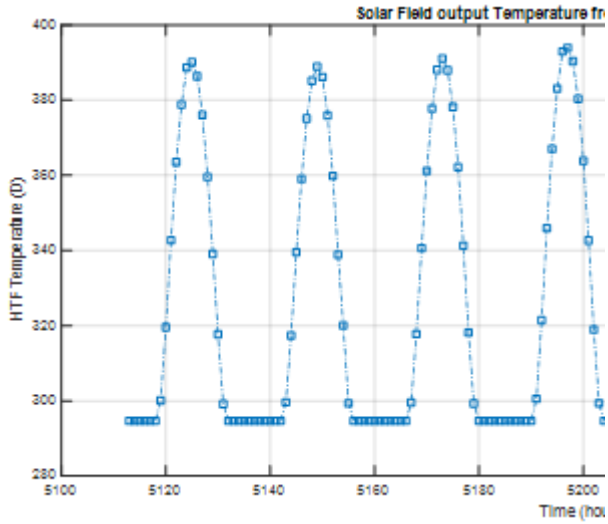

Figure 6 and

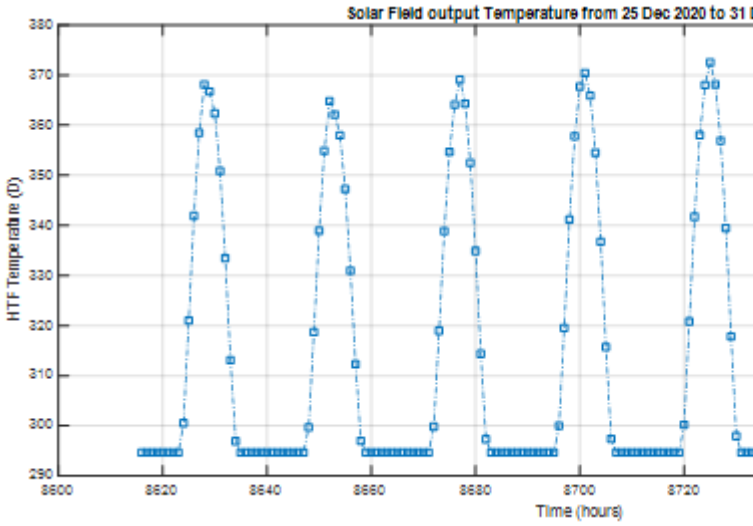

Figure 7 Show the Solar field output temperature through the first week of August, and the last week of December.

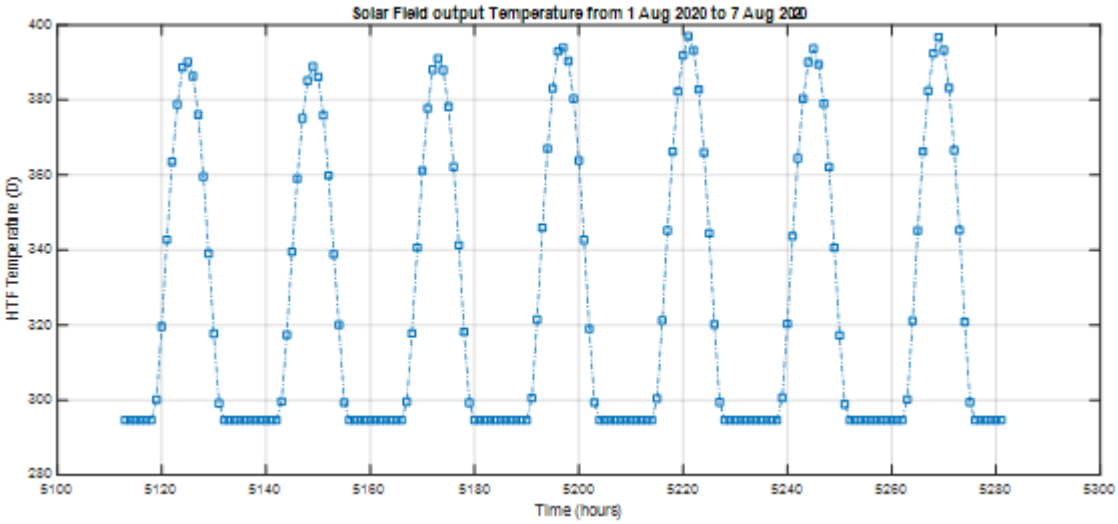

Figure 6: Solar field output temperature through the first week of August

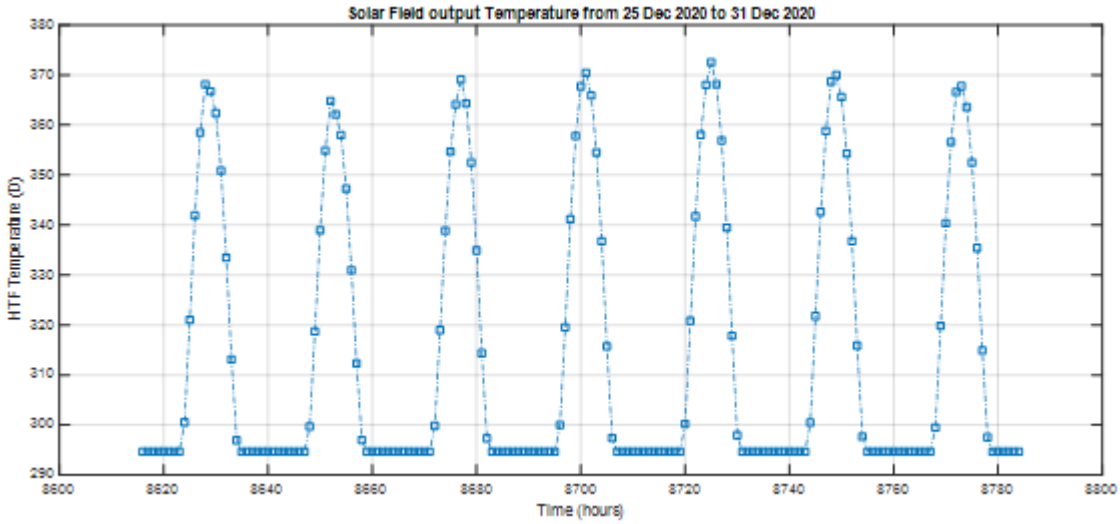

Figure 7: Solar field exit temperature through the last week of December

7. Design and modeling of the integrated power block with Double Reheat and Feed Water Heaters

Power generation system analyses are of scientific interest and crucial to the efficient use of energy resources. The first law of thermodynamics is the technique most often employed to analyze an energy conversion process. A mechanism for clearly differentiating between energy losses to the environment and internal irreversibility in the process is provided by exergetic analysis [22]. The first law of thermodynamics, on which energy analysis is predicated, has several intrinsic limitations, such as not taking into consideration system environment characteristics or the deterioration of energy quality due to dissipative processes. The irreversibility of system processes is not characterized by an energy analysis. Exergy analysis, on the other hand, will describe a system's ability to produce work. When a system is brought to a reference or dead state, its exergy is the greatest amount of work that can be gained from it [23].

Both the ambient temperature and the direct normal Irradiation for Makkah city is used as the input for the corresponding power block's performance calculation and analysis. In order to investigate the impact of direct solar irradiation on the power output and efficiency of the solar electric generating system.

The Power block is directly integrated with the output of the solar filed there for this section will demonstrate the performance of the cycle with the solar irradiance changes though out the day.

The essential components of this cycle are a boiler, a turbine, a condenser, feed water heaters, a deaerator, a feed water pump, and an extraction pump. The suggested power cycle structure can be seen in Figure 8.

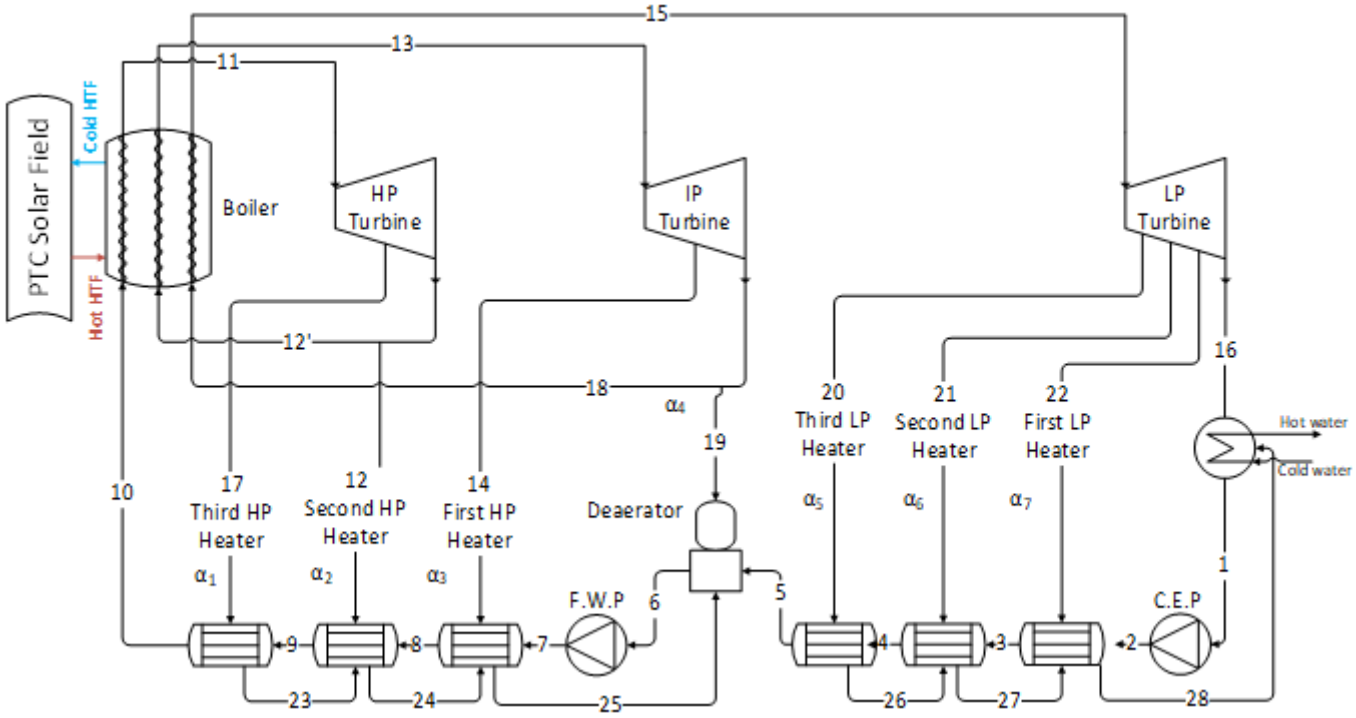

Figure 8: Schematic of the proposed Power cycle

Table 4: Process parameters of the CSP integrated power cycle at $T_{field\ out} = 390$ ℃.

Point	$T(^{\circ}C)$	$P(kpa)$	$h(kJ/kg)$	$s(kJ/Kkg)$	$\dot{m}(kg/s)$	$\psi(kJ/kg)$
1	45.80	1199	191.8123	0.649218	27.78128	2.85088
2	45.87	1199	193.0135	0.64936	27.78128	4.009733
3	85.91	1199	360.7721	1.144298	27.78128	24.18737
4	107.52	1199	451.658	1.390389	27.78128	41.82715
5	131.11	15000	551.7275	1.645537	27.78128	65.85775
6	132.11	15000	556.0568	1.656069	43.3	66.98024
7	133.61	15000	588.8453	1.658348	43.3	82.0127
8	196.81	15000	1028.189	2.28055	43.3	168.9668
9	242.78	15000	1306.632	2.702515	43.3	251.277
10	243.87	4153.5	1308.087	2.712429	43.3	253.4449
11	390	4153.5	1956.063	5.816644	43.3	1203.255
12	252.60	1638.473	1885.794	5.889896	5.04445	963.1881
12’	390	1199	1885.794	6.715045	32.66985	1191.228
13	272.02	10	3104.481	6.759745	2.441254	960.6413
14	390	7560.4	2902.677	7.347448	27.78128	1054.76
15	45.80	1199	3239.951	7.633233	24.13975	149.2156
16	299.80	1199	2419.497	5.854357	5.58137	1070.061
17	237.60	327.69	1922.489	6.77687	27.78128	892.2972
18	237.60	141.482	2722.989	6.77687	2.441254	892.2972
19	234.61	64.99	2722.989	7.415121	1.13446	730.4233
20	154.43	7560.49	2935.746	7.469886	0.903671	560.9411
21	91.67	4153.5	2782.701	7.524585	1.6021	425.8954
22	250.78	1638.47	2663.811	2.792018	5.58137	262.0304
23	204.81	327.6	1357.979	2.372189	10.63015	172.6612
24	170.52	141.48	1060.939	2.046014	13.07227	116.6606
25	115.52	64.99	862.3036	1.479096	1.13446	48.57819
26	93.91	1199	484.8437	1.237717	2.038131	29.15987
27	53.87	1199	393.5838	0.753565	3.640231	5.480551
28	45.80	1199	225.5385	0.649218	27.78128	2.85088
Cold water	25	101	104.8	0.3669	27.78128	0
Hot Water	35	101	146.7	0.5049	27.78128	0.7069

In this study, energy and exergy analysis is carried out to assess the performance of the steam power plant cycle proposed above employing six closed feed water heaters with double reheat and various extraction pressures. In order to establish the first and second law efficiency under various operating situations, a parametric research is conducted after identifying the sources of exergy destruction in the power plant. At the ideal extraction pressure, maximum first law efficiency is attained.

The first law of thermodynamics has the following form for an open system in steady state: [24-26]

$$\sum \dot{Q} + \dot{m}\left(h_i + \frac{v_i^2}{2} + gz_i\right) = \dot{m}\left(h_o + \frac{v_o^2}{2} + gz_o\right) + W \quad (22)$$

There are two ways to define the power cycle's energy efficiency. Physical exergy is the first, while chemical exergy is the second. The kinetic and potential components of exergy are regarded as insignificant in this work. Since the power cycle is designed on no combustion fuel The chemical reactions of stoichiometric combustion are assumed to be negligible.

The exergy destroyed rate and the exergy at any state of an open system are generally shown by equations (26) and (27):

$$\dot{E}x_Q + \sum_{in} \dot{m}_i ex_i = \sum_{out} \dot{m}_o ex_o + \dot{E}x_W + \dot{E}x_D \quad (23)$$

$$\dot{E}x_Q = \left(1 - \frac{T_o}{T_k}\right)\dot{Q}_k \quad (24)$$

$$\dot{E}x_W = \dot{W} \quad (25)$$

$$\dot{E}x = \dot{E}x_{ph} + \dot{E}x_{ch} \quad (26)$$

$$\dot{E}x_{ph} = \dot{m}[(h - h_o) - T_o(s - s_o)] \quad (27)$$

Where the subscript T is the absolute temperature (K), (0) denotes the ambient condition, and $\dot{E}x_Q, \dot{E}x_W$, and $\dot{E}x_D$ are the equivalent exergy of heat transfer, work, and exergy destruction that cross the limits of the control volume. The following are the equations for energy and exergy destroyed for the main component of the cycle.

The Turbine.

$$\begin{aligned}\dot{w}_t = \{&\dot{m}_{11}(h_{11} - h_{17}) + (\dot{m}_{10} - \alpha_1)(h_{17} - h_{12}) \\ &+ (\dot{m}_{10} - \alpha_1 - \alpha_2)(h_{13} - h_{14}) \\ &+ (\dot{m}_{10} - \alpha_1 - \alpha_2 - \alpha_3)(h_{14} - h_{18}) \\ &+ (\dot{m}_{10} - \alpha_1 - \alpha_2 - \alpha_3 - \alpha_4)(h_{15} - h_{20}) \\ &+ (\dot{m}_{10} - \alpha_1 - \alpha_2 - \alpha_3 - \alpha_4 - \alpha_5)(h_{20} - h_{21}) \\ &+ (\dot{m}_{10} - \alpha_1 - \alpha_2 - \alpha_3 - \alpha_4 - \alpha_5 - \alpha_6)(h_{21} - h_{22}) \\ &+ (\dot{m}_{10} - \alpha_1 - \alpha_2 - \alpha_3 - \alpha_4 - \alpha_5 - \alpha_6 - \alpha_7)(h_{22} - h_{16})\},\end{aligned} \quad (28)$$

$$\begin{aligned}\dot{I}_t = \{&-T_o[\dot{m}_{11}(s_{11} - s_{17}) + (\dot{m}_{10} - \alpha_1)(s_{17} - s_{12}) \\ &+ (\dot{m}_{10} - \alpha_1 - \alpha_2)(s_{13} - s_{14}) \\ &+ (\dot{m}_{10} - \alpha_1 - \alpha_2 - \alpha_3)(s_{14} - s_{18}) \\ &+ (\dot{m}_{10} - \alpha_1 - \alpha_2 - \alpha_3 - \alpha_4)(s_{15} - s_{20}) \\ &+ (\dot{m}_{10} - \alpha_1 - \alpha_2 - \alpha_3 - \alpha_4 - \alpha_5)(s_{20} - s_{21}) \\ &+ (\dot{m}_{10} - \alpha_1 - \alpha_2 - \alpha_3 - \alpha_4 - \alpha_5 - \alpha_6)(s_{21} - s_{22}) \\ &+ (\dot{m}_{10} - \alpha_1 - \alpha_2 - \alpha_3 - \alpha_4 - \alpha_5 - \alpha_6 - \alpha_7)(s_{22} - s_{16})]\},\end{aligned} \quad (29)$$

$$\eta_{II,t} = \frac{\dot{w}_t}{\dot{I}_t + \dot{w}_t} \quad (30)$$

The Boiler.

$$\begin{aligned}\dot{q}_B = &\dot{m}_{11}h_{11} - \dot{m}_{10}h_{10} + (\dot{m}_{10} - \alpha_1 - \alpha_2)(h_{13} - h_{12'}) \\ &+ (\dot{m}_{10} - \alpha_1 - \alpha_2 - \alpha_3 - \alpha_4)(h_{15} - h_{18}),\end{aligned} \quad (31)$$

$$\begin{aligned}\dot{I}_B = \{&\dot{m}_{10}(h_{10} - h_{11}) + (\dot{m}_{10} - \alpha_1 - \alpha_2)(h_{12'} - h_{13}) \\ &+ (\dot{m}_{10} - \alpha_1 - \alpha_2 - \alpha_3 - \alpha_4)(h_{18} - h_{15}) \\ &-T_o[(s_{10} - S_{11}) + (\dot{m}_{10} - \alpha_1 - \alpha_2)(s_{12'} - s_{13})] \\ &+ (\dot{m}_{10} - \alpha_1 - \alpha_2 - \alpha_3 - \alpha_4)(s_{18} - s_{15})]\} \\ &+ \dot{q}_B\left(1 - \frac{T_o}{T_B}\right)\end{aligned} \quad (32)$$

$$\eta_{II,B} = \frac{\dot{I}_t}{Ex_{in}} \quad (33)$$

The Condenser.

$$\begin{aligned}\dot{q}_c = &\ (\dot{m}_{10} - \alpha_1 - \alpha_2 - \alpha_3 - \alpha_4 - \alpha_5 - \alpha_6 - \alpha_7)h_{16} \\ &+(\alpha_5 - \alpha_6 - \alpha_7)h_{28} - (\dot{m}_{10} - \alpha_1 - \alpha_2 - \alpha_3 - \alpha_4)h_1,\end{aligned} \quad (34)$$

$$\dot{I}_c = \{(\dot{m}_{10} - \alpha_1 - \alpha_2 - \alpha_3 - \alpha_4 - \alpha_5 - \alpha_6 - \alpha_7)h_{16} + (\alpha_5 - \alpha_6 - \alpha_7)h_{28} - (\dot{m}_{10} - \alpha_1 - \alpha_2 - \alpha_3 - \alpha_4)h_1\} - T_o\{(\dot{m}_{10} - \alpha_1 - \alpha_2 - \alpha_3 - \alpha_4 - \alpha_5 - \alpha_6 - \alpha_7)s_{16} + (\alpha_5 - \alpha_6 - \alpha_7)s_{28} - (\dot{m}_{10} - \alpha_1 - \alpha_2 - \alpha_3 - \alpha_4)s_1\} + \dot{m}_{w,\text{in}}\{(h_{w,\text{in}} - h_{w,\text{out}}) - T_o(s_{w,\text{in}} - s_{w,\text{out}})\} \quad (35)$$

$$\eta_{\text{II},c} = \frac{\dot{I}_t}{\psi_{in,\text{C}}} \quad (36)$$

The Condensate Extraction Pump

$$\dot{w}_{C.E.P} = (\dot{m}_{10} - \alpha_1 - \alpha_2 - \alpha_3 - \alpha_4)(h_2 - h_1), \quad (37)$$

$$\dot{I}_{C.E.P} = \{(\dot{m}_{10} - \alpha_1 - \alpha_2 - \alpha_3 - \alpha_4) \times \{(h_1 - h_2) - T_o(s_1 - s_2)\} + |\dot{w}_{C.E.P}|, \quad (38)$$

$$\eta_{\text{II,C.E.P}} = 1 - \frac{\dot{I}_{\text{C.E.P}}}{\dot{w}_{C.E.P}}. \quad (39)$$

The Feed water pump

$$\dot{w}_{\text{F.W.P}} = \dot{m}_7(h_7 - h_6), \quad (40)$$

$$\dot{I}_{C.E.P} = \dot{m}_7\{(h_6 - h_7) - T_o(s_6 - s_7)\} + |\dot{w}_{F.W.P}|, \quad (41)$$

$$\eta_{\text{II,F.W.P}} = 1 - \frac{\dot{I}_{\text{F.W.P}}}{\dot{w}_{\text{F.W.P}}}. \quad (42)$$

The definition of energy efficiency (thermal efficiency) is

$$\eta_{\text{thermal}} = \frac{\dot{W}_{\text{Net}}}{\dot{Q}_{\text{B}}}. \quad (43)$$

Where it is clear that

$$\dot{W}_{\text{Net}} = \dot{W}_{\text{T}} - \dot{W}_{\text{C.E.P}} - \dot{W}_{\text{F.W.P}}. \quad (44)$$

Ex_{in} is the system's intake Exergy balance equations and is stated by Petela [27] to be a function of the sun's outer surface temperature (Ts = 5800 K).

$$Ex_{\text{in}} = A_{ap,t}G_b\left(1 + \frac{1}{3}\left(\frac{T_o}{T_s}\right)^4 - \frac{4}{3}\left(\frac{T_o}{T_s}\right)\right) \quad (45)$$

While exergy efficiency (the second law's definition of efficiency) is defined as the ratio of the actual thermal efficiency to the maximal reversible thermal efficiency when both are present. The following are the definitions of the terms:

$$\eta_{\text{exe}} = \frac{\dot{W}_{\text{Net}}}{Ex_{\text{in}}} \quad (46)$$

Table 5: Power balance between the main parts of the power plant

Component	Power balance (kW)	Exergy destruction (kw)
Boiler	115864.60	69719.03
Condenser	95472.52	6249.9
Turbines	55977.26	5389.9
Feed water pump	680.31	29.4
Condense extraction pump	51.58	1.81

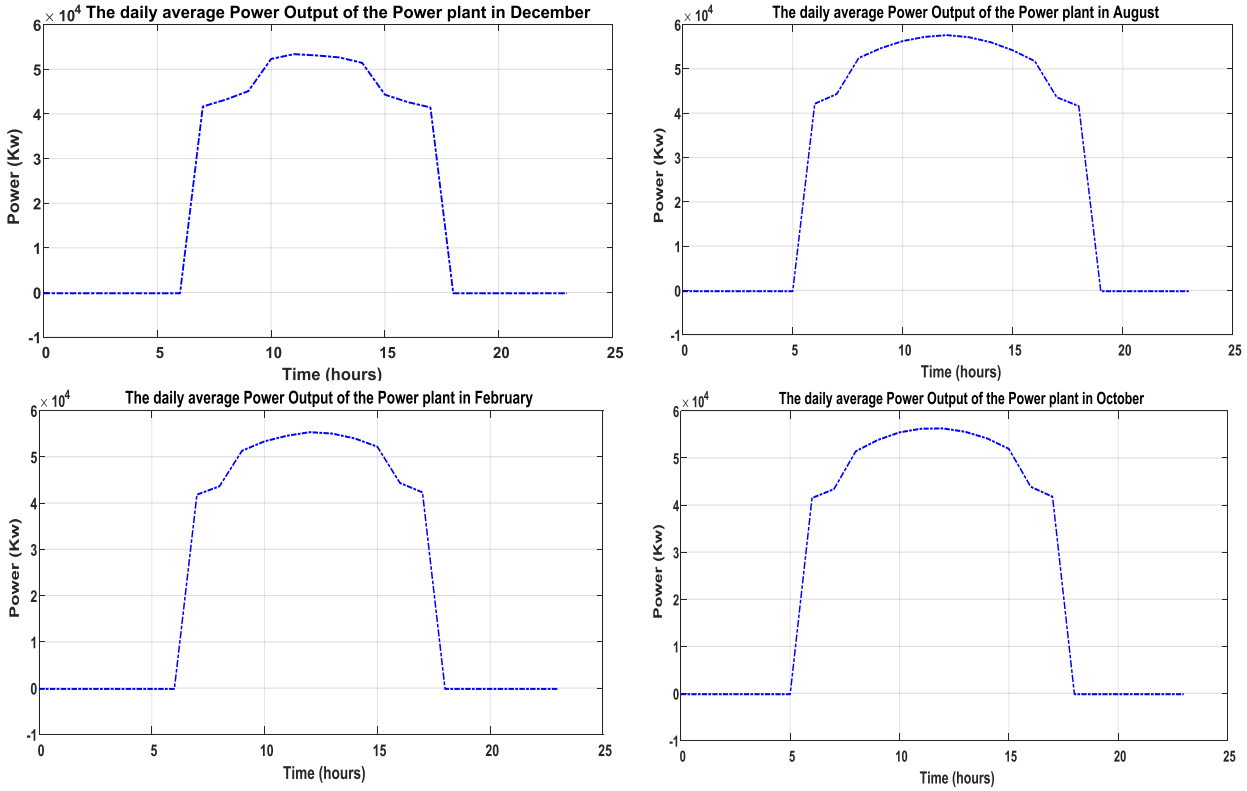

Figure 9: Daily average Power output for several months in 2020

Plant Numerical Modeling Using MATLAB

The primary analysis tool used to evaluate all the plant performance for this study is MATLAB®. There are other specialized tools can be used for this kind of analysis such as TRANSYS, Engineering equation solver (EES), However the researchers decide to use MATLAB® for several reasons:

- MATLAB® is more detailed analysis tool which will enhance the researcher experience in writing every component details. Where on the other hand, other tool could provide a closed accessed plant pre-written code which limit the researcher experience to enter the input values with little modification range.
- It is licensed by Umm Al-Qura University for facility and students, which lower the required funds for the presented study.
- The main author of this study has a previous experience with MATLAB®, which will reduce the required learning time for the plant analysis.

The MATLAB modelling script for the proposed plant analysis is divided into two sections. The first section is responsible for extracting the solar data from an excel file for the year of 2020, in addition to collector parameters and specifications and calculating the field losses, angles, all the way through to the solar field outlet temperature, efficiency, and heat rate as illustrated in

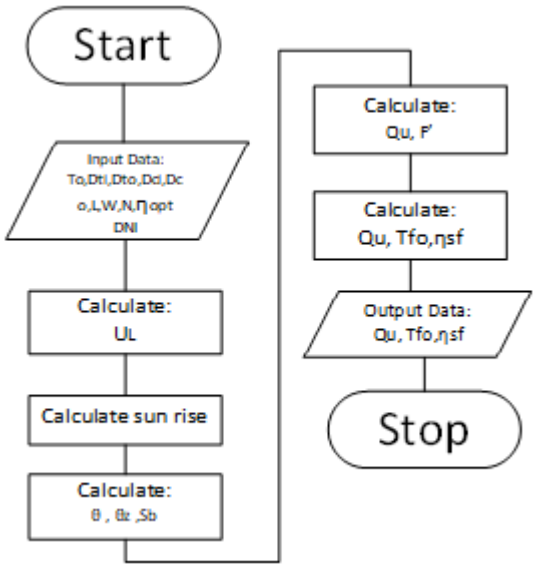

Figure 10: Flow chart of the Solar Field Model

Since all the solar DNI inputs is directly imported from an excel file containing 1 year of hourly measurements of Makkah city 2020 solar data. And collector specifications such as pipes and mirror geometry is based on LS-3 product sheet [21].

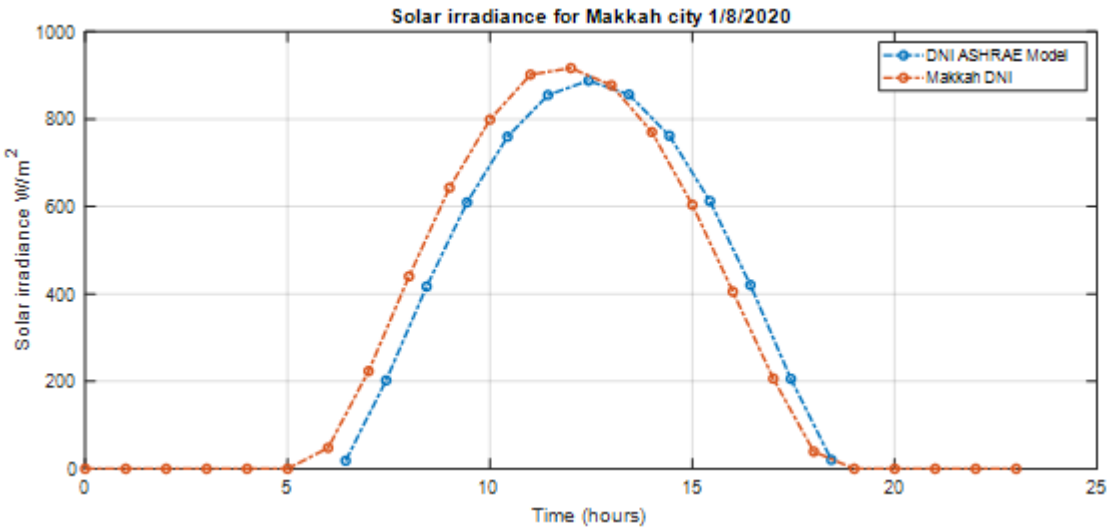

Figure 11: Comparison between DHI ASHRAE Model and DNI Actual data on 1/8/2020

The validation for the solar data is done by comparing the Ashrae model solar results for the same location with the actual measured DNI as demonstrated in Figure 17 and Figure 18, to make sure that the registered data is accurate and acceptable. Moreover, the ashre model can be used as a primary prediction source for solar data if there is no pre-recorded solar data by installed station.

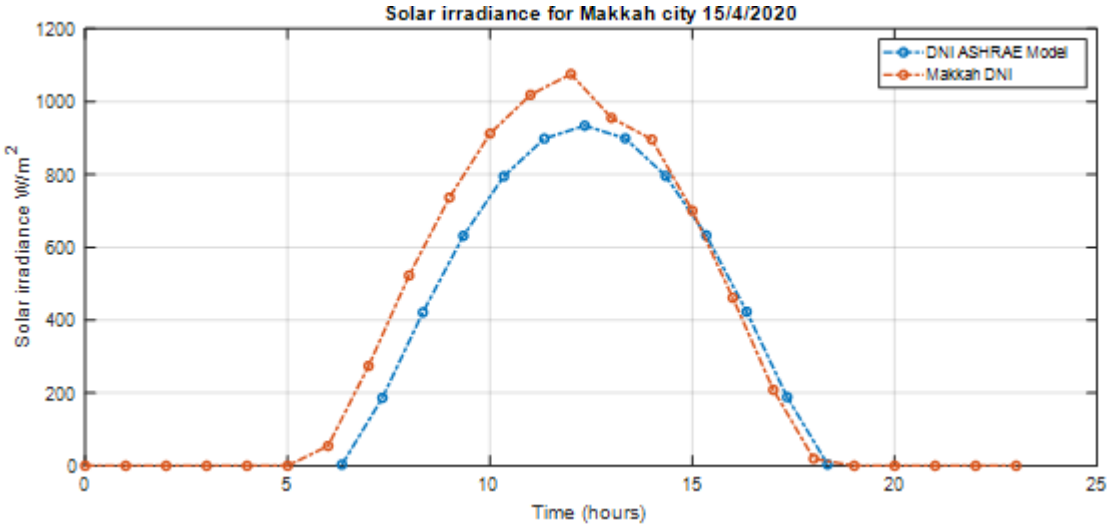

Figure 12: Comparison between DHI ASHRAE Model and DNI Actual data on 1/4/2020

The proposed power block described in this work has been programmed fully using MATLAB live script. The initial input to begin the cycle flow chart in Figure 19 is divided into two groups. First, Solar inputs, which depends mainly on the solar filed outlet temperature. Second, the assumption, component efficiency, and the ambient conditions.

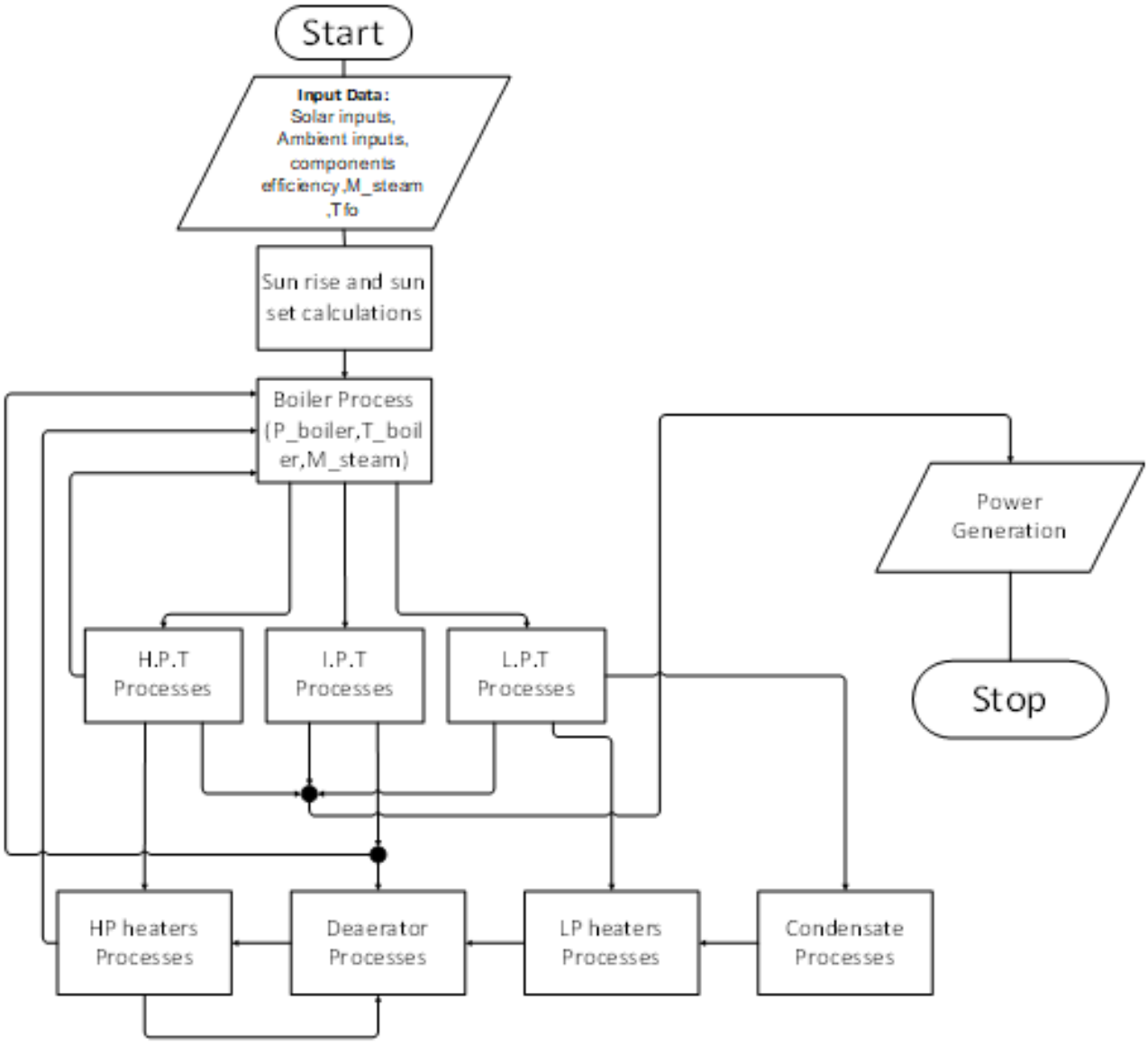

Figure 13: Flow chart of the proposed power block

The power cycle will be running when enough solar energy is supplied to run the designed 50 MW power cycle, therefore, since no thermal storage condition is applied the amount of thermal energy needed is in range of 115-130 MW, and the temperature needed to start the power cycle is 390 ˚C.

Right after this condition is satisfied then a function named (X steam) is then used to calculate point states enthalpy, entropy, pressure, temperature, and other thermodynamic properties through the thermodynamic correlation equations [28].

The components efficiency and ambient assumptions is listed in Table 6

Table 6: Inputs utilized in the proposed power cycle[29]

Turbines efficiency		Ambient parameters	
LPT	0.9	Air Temp.	25 ˚C
IPT	0.9	pressure	101.3 kPa
HPT	0.85		
Cycle assumptions			
Mass flow rate	43.3 kg/s	**Extraction lines mass flow rate percentage**	
		a1=12.8%	a4=5.63%
Cooling water mass flow rate	32.65 kg/s	a2=11.6%	a5=2.62%
Approach temperature	8 ˚C	a3 =5.63%	a6=2.08%
		a7=3.70%	

8. Results and Discussion

The effect of variations in sun irradiation on plant performance should be the primary factor considered when developing a solar thermal power plant. Variation in the solar field output temperature is another important factor to consider when evaluating its heat transfer fluid volumetric flow rate and its properties on power plant energetic performance. The suggested solar field design's performance was evaluated. The output thermal power and the mass flow rate of the heat transfer fluid rise when the solar radiation increases, as can be observed in Figure 9 and Figure 10. Due to thermal losses from the field, the heat transfer fluid captures about 65% of the energy that the solar collector element receives from the sun.

Another crucial factor in the system's energetic performance is analyzing the effects of changing the net electric power output, which in turn affects the size of the solar field. By changing the steam mass flow rate, the steam Rankine cycle's net electrical power output can be changed. As a result, it was determined how these three variables affected the systems under consideration's exergetic performance. The systems under consideration had their exergetic and energetic performance thoroughly assessed at the variation of Makkah citysolar irradiation intensity to provide constant 50MW in the daytime. Additionally, the impact of daytime sun irradiation on the systems under consideration was investigated. A wide range of solar intensities, Gb = 0.6-1.1$\frac{kW}{m^2}$as in **Error! Reference source not found.**, were taken into account. And Thermodynamic characteristics for the integrated power block with receiving an average of Gb0.9kW/m^2solar irradiation intensity and standard conditions of $T_{field\ out} = 390\ ℃$.

A critical decision is choosing an aperture area that is appropriate for the full load functioning. While a small aperture area will mostly be adequate on the summer and just partially the rest of the year. The total aperture area required to give the needed thermal energy to produce 50MW is 246, 885m^2 it was calculated at the least solar irradiance of 2020 with peak $Q_{absorbed}$ = 450, 2 W/m^2, which was in 31st of December to ensure 50MW will be supplied even when DNI decrease as shown in Figure 9, that also will results in more than 50MW during summer season around 5MW surplus will be produced, by using the LS-3 solar field properties and operating conditions, shown in Table 2 and Table 3.

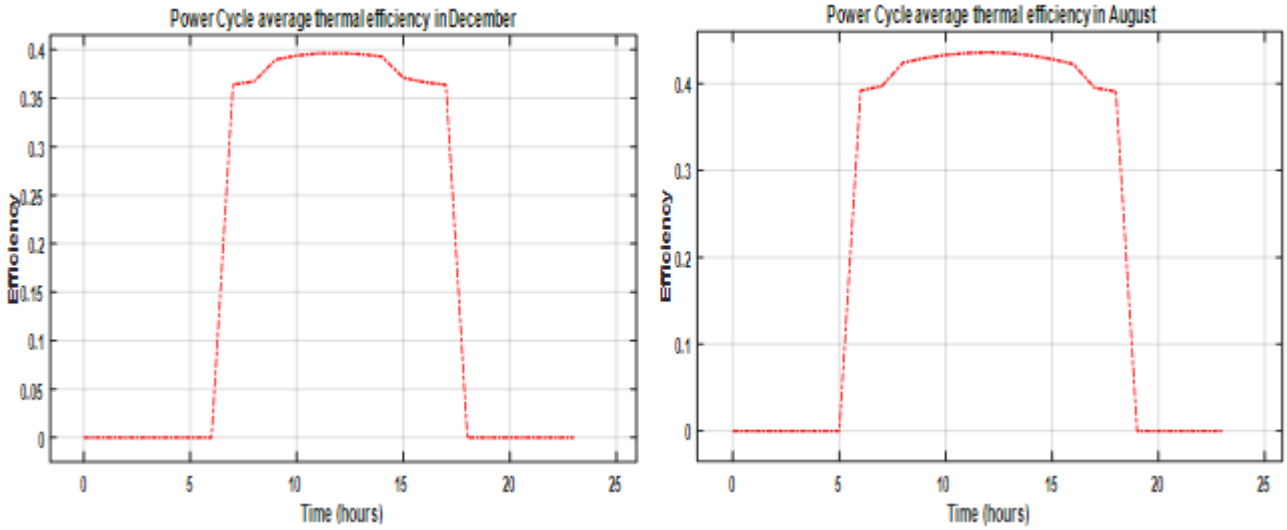

Figure 20: Average Power cycle efficiency in August and December 2020

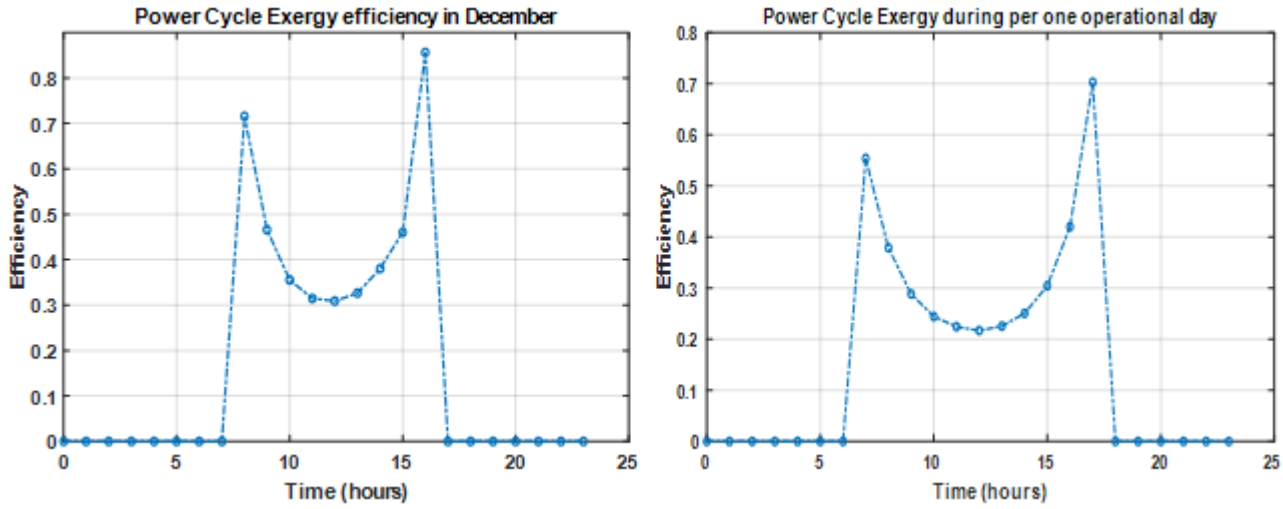

Figure 14: Average Power cycle exergy efficiency in August and December 2020

The efficiency, DNI, and daily power output have all been examined. The gross electrical power output and efficiency are shown in Figure 9 and

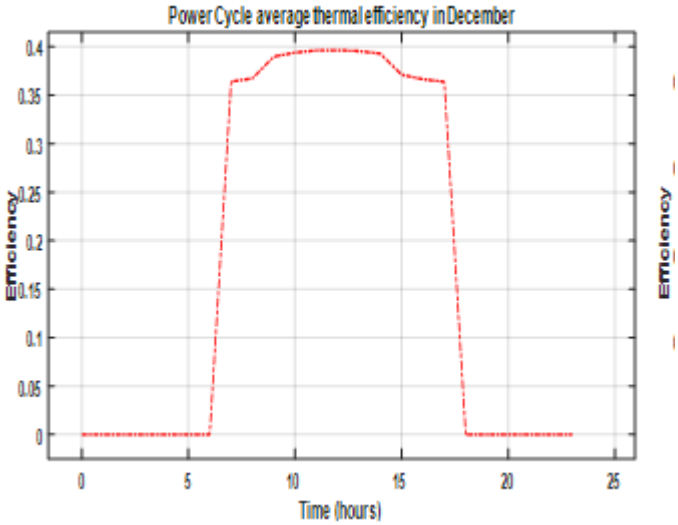

Figure for various picked months throughout the year. Clearly, when there is more solar radiation, the plant's gross output is maximum such is the case in summer season.

Exergetic assessment of the key elements of the Power block taken into consideration was used to conduct the exergetic analysis. The exergetic assessment considered important exergy parameters such the rate at which exergy is destroyed and the potential for exergy improvement, as illustrated in Table 4, Table 5. These parameters' values are based on standard operating procedures: the net electrical power is 50 MW, Gb = 0.9kW/m^2, and the steam turbine's inlet pressure is 15 MPa.

Table 5 displays the exergy destruction rate and

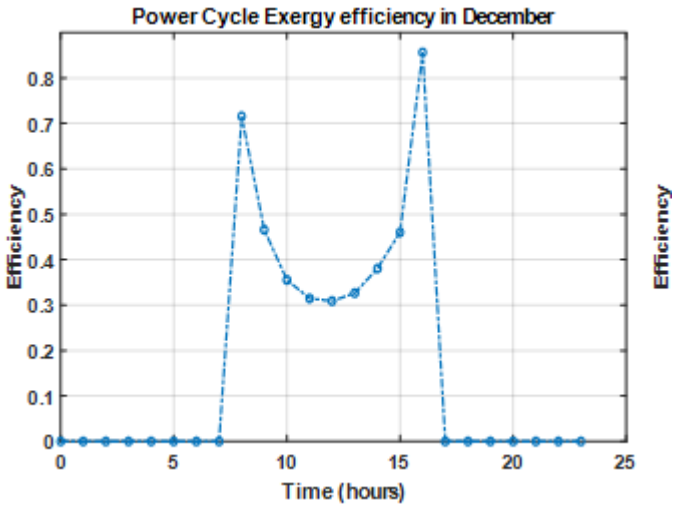

Figure 14 demonstrate the exergy efficiency for the power system. The solar collectors, which have a exergy destruction rate of 69, 719 kW, were shown to be the primary cause of exergy destruction. This significant exergy destruction is mostly caused by the collector's huge temperature differential. The condenser comes in second with 6249.9 kW, followed by the steam turbines with 5389.9 kW as other major causes of exergy destruction.

9. Conclusion

Increasing the production of renewable energy is one of Saudi Arabia's strategic goals, and it is apparent that renewable energy plants and technologies, like CSP plant, is nowadays a significant concern for the majority of global countries, particularly those based in the MENA area. It became one of the top 2030 vision targets due to the increase in oil costs, the energy crisis, and other issues. Investigations are conducted on the first and second laws of the cycle's thermal and exergy efficiency. According to the findings, an LS-3 collector type with an aperture size of 246, 885 m^2 and a full plant area of 976, 416 m^2 can produce 117.2 GWh of power annually, which is equivalent to saves an amount of 83, 058 metric tons of Carbon Dioxide (CO_2). Additionally, as most Sun-built regions, including the MENA countries, have average DNI numbers higher than the commercially acceptable average yearly direct normal irradiation (DNI) of 2000 kWh/m^2, it is feasible to operate CSPP there. The use of CSPP may not only lead to the creation of jobs, but it may also serve to lessen the risk of disputes over energy. Additionally, this technology might significantly contribute to the reduction of greenhouse gas emissions.

Author Contributions

Conceptualization, Talal Alsufyani; Investigation, Talal Alsufyani; Methodology, Talal Alsufyani; Supervision, Abdulmajeed Al-Ghamdi ; Writing – original draft, Talal Alsufyani; Writing – review & editing, Talal Alsufyani and Abdulmajeed Al-Ghamdi .

References

[1] KAPSARC, K.A.P.S. *Changing Energy Supply Economics in Saudi Arabia in the Context of Global Transitions*. in *Workshop Briefs*. 2020. King Abdullah Petroleum Studies and Research Center.

[2] Matar, W. and A.M. Elshurafa, *Electricity transmission formulations in multi-sector national planning models: An illustration using the KAPSARC energy model.* Energy Reports, 2018. **4**: p. 328-340.

[3] Lippke, F., *Simulation of the part-load behavior of a 30 MWe SEGS plant*. 1995, Sandia National Lab.(SNL-NM), Albuquerque, NM (United States).

[4] Woditsch, P., *Kostenreduktionspotenziale bei der Herstellung von PV-Modulen.* Proceedings of FVS Themen, 2000: p. 72-86.

[5] Yadav, S.K. and U. Bajpai, *Performance evaluation of a rooftop solar photovoltaic power plant in Northern India.* Energy for Sustainable Development, 2018. **43**: p. 130-138.

[6] Price, H.W. and S. Carpenter, *The potential for low-cost concentrating solar power systems*. 1999, National Renewable Energy Lab.(NREL), Golden, CO (United States).

[7] Patnode, A.M., *Simulation and performance evaluation of parabolic trough solar power plants.* 2006.

[8] Kopp, J.E., *Two-tank indirect thermal storage designs for solar parabolic trough power plants*. 2009, University of Nevada, Las Vegas.

[9] Masdar. *Shams 1 CSP solar station*. 2022 [cited 2022 June 24th]; Available from: https://masdar.ae/ar/Masdar-Clean-Energy/Projects/Shams.

[10] *TSK 50 MW SHAGAYA CSP Plant*. 2018 [cited 2021 Nov 11]; Available from: https://www.grupotsk.com/en/proyecto/50-mw-shagaya-csp-plant/.

[11] company, A. *Dubai, UAE Noor Energy 1 P.S.C energy solar station*. 2022 [cited 2022 July 24th]; Available from: https://acwapower.com/en/projects/noor-energy-1/.

[12] Zell, E., et al., *Assessment of solar radiation resources in Saudi Arabia*. Solar Energy, 2015. **119**: p. 422-438.

[13] Trieb, F. *Global potential of concentrating solar power*. in *Conference Proceedings*. 2009.

[14] Company, E.C. *Liquid properties of Therminol VP-1 heat transfer fluid by temperature*. 2022 [cited 2022 June 20th]; Available from: https://www.therminol.com/product/71093459.

[15] Padilla, R.V., *Simplified methodology for designing parabolic trough solar power plants*. 2011: University of South Florida.

[16] Limited, L.I., *Solar electric generating system IX technical description*. 1990, LUZ International Limited Los Angeles, CA.

[17] Lotker, M., *Barriers to commercialization of large-scale solar electricity: Lessions learned from the LUZ experience*. 1991, Sandia National Lab.(SNL-NM), Albuquerque, NM (United States).

[18] Gilman, P., et al., *Solar Advisor Model User Guide for Version 2.0*. 2008.

[19] Duffie, J.A. and W.A. Beckman, *Solar engineering of thermal processes*. 1980: Wiley New York.

[20] Mokheimer, E.M., et al., *Techno-economic performance analysis of parabolic trough collector in Dhahran, Saudi Arabia.* Energy conversion and management, 2014. **86**: p. 622-633.

[21] Dudley, V.E., et al., *Test results: SEGS LS-2 solar*

collector. 1994, Sandia National Lab.(SNL-NM), Albuquerque, NM (United States).

[22] Kopac, M. and A. Hilalci, *Effect of ambient temperature on the efficiency of the regenerative and reheat Çatalağzı power plant in Turkey.* Applied Thermal Engineering, 2007. **27**(8-9): p. 1377-1385.

[23] Regulagadda, P., I. Dincer, and G. Naterer, *Exergy analysis of a thermal power plant with measured boiler and turbine losses.* Applied Thermal Engineering, 2010. **30**(8-9): p. 970-976.

[24] Cengel, Y.A., M.A. Boles, and M. Kanoğlu, *Thermodynamics: an engineering approach*. Vol. 5. 2011: McGraw-hill New York.

[25] Bejan, A., G. Tsatsaronis, and M. Moran, *Thermal design and optimization Wiley*. 1996, Interscience: New York USA.

[26] Kaushik, S., V.S. Reddy, and S. Tyagi, *Energy and exergy analyses of thermal power plants: A review.* Renewable and Sustainable energy reviews, 2011. **15**(4): p. 1857-1872.

[27] Petela, R., *Exergy analysis of the solar cylindrical-parabolic cooker.* Solar Energy, 2005. **79**(3): p. 221-233.

[28] Holmgren, M., *X steam for matlab.* www. x-eng. com, accessed October, 2006. **21**: p. 2006.

[29] Rashidi, M., A. Aghagoli, and M. Ali, *Thermodynamic analysis of a steam power plant with double reheat and feed water heaters.* Advances in Mechanical Engineering, 2014. **6**: p. 940818.